Stateless Linear-path Routing for 3D Nanonetworks

Angeliki Tsioliaridou
FORTH, Greece
atsiolia@ics.forth.gr

Christos Liaskos
FORTH, Greece
cliaskos@ics.forth.gr

Eugen Dedu
FEMTO-ST, France
eugen.dedu@univ-fcomte.fr

Sotiris Ioannidis
FORTH, Greece
sotiris@ics.forth.gr

ABSTRACT

Efficient data routing is a critical enabler of future nanonetworking applications. Such nano-routing schemes must account for highly lossy wireless channel conditions, non-unique identifiers and limited processing capabilities at the nanonodes comprising the network. The present study proposes a novel addressing and routing scheme fit for 3D nanonetworks. Initially, a geo-addressing process is applied within the network. Subsequently, it is shown that every node can deduce whether it is located on the linear path connecting a communicating node-pair. This deduction is made using integer calculations, node-local information and in a stateless manner, minimizing the computational and storage overhead of the proposed scheme. Most importantly, the nodes can regulate the width of the linear path, thus trading energy efficiency (redundant transmissions) for increased path diversity. This trait can enable future adaptive routing schemes. Extensive evaluation via simulations highlights the advantages of the novel scheme over related approaches.

Keywords

Electromagnetic nano-networking, multi-hop communication.

1. INTRODUCTION

Nanonetworking is expected to enable ground-breaking applications in several sectors, such as medicine, and the materials industry [2]. Nonetheless, the required miniaturization of electronic components poses new challenges at physical, networking and application layers. This paper focuses on the networking layer and studies the open research issues of nano-node addressing and data routing. The explicit scope of the proposed solutions is large networks of immobile nodes, which exchange data via multi-hop routing. Such networks can find applications within Software-defined Materials (SDMs), which can receive external commands and tune their electromagnetic and mechanical behavior accordingly [3, 14]. SDMs can be programmed to serve as perfect absorbers or reflectors of electromagnetic energy and light, maximizing the efficiency of renewable energy sources.

Physical manufacturing limitations at nano-scale requires unique nano-addressing and nano-routing solutions [22]. First, the power supply units of autonomous nano-nodes can scavenge energy for 1 packet transmission per approximately 10 sec [8]. Second, the wireless nano-communication modules are expected to operate at the THz band, which translates to highly lossy channel conditions due to acute molecular absorption phenomena [22]. Third, manufacturing restrictions and cost considerations correspond to "weak" nano-node hardware, i.e., limited CPU and data storage capabilities [2]. The impact of these restrictions on nano-node addressing is that assigning unique identifiers to each node is not scalable, mainly due to power restrictions. Regarding data routing, on the other hand, the expectedly frequent transmission failures require a mechanism to balance path redundancy and energy consumption, while incurring low computational complexity and memory overhead [22].

The present paper contributes a routing and addressing scheme for 3D nano-networks that respects the posed restrictions. The addressing part can be classified as a geo-addressing scheme and extends the authors' past work from 2D to 3D [20]. A stateless routing scheme is proposed, which runs on top of the addressing scheme. According to it, a node can deduce whether it is located on the line connecting the packet sender to the packet destination. The scheme offers tunable path redundancy by controlling the width of the 3D line, which constitutes its major advantage over related solutions [20]. Additionally, it requires node-local information and integer computations only, respecting the nano-CPU limitations. Finally, due to its stateless nature, it does not require routing tables for its operation and, hence, no permanent storage either.

The remainder of this paper is organized as follows. Sections 2 and 3 introduce the proposed 3D addressing concept and the novel routing scheme, respectively. Evaluation via simulations takes place in Section 4. Related studies are given in Section 5. Finally, Section 6 draws the conclusion.

2. NANONODE ADDRESSING IN 3D

Figure 1 illustrates the considered system setup, comprising a set of nanonodes placed within a 3D rectangular *network space*. The layout of the nodes is either a regular grid or random within the space. The grid setup corresponds to an active meta-material application, while the random placement to a smart material monitoring setup [14]. The

NANOCOM'16, September 28-30, 2016, New York, NY, USA

DOI: http://dx.doi.org/10.1145/2967446.2967451

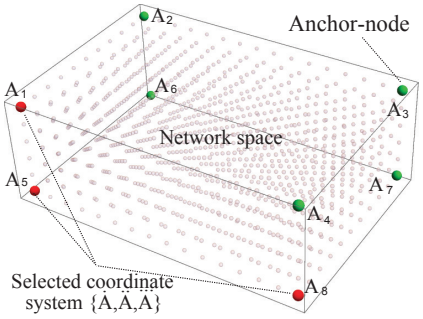

Figure 1: Overview of the studied nanonetwork.

network nodes have the same hardware, and a short wireless connectivity radius imposed by the nature of the application [14]. Therefore, we assume a multi-hop packet routing case, with identical transmission distance. Additionally, the network conditions are such that node failures are common, accentuating the need for alternative paths (path redundancy). Nanonode communication may temporarily fail due to error-prone hardware, battery depletion or channel conditions [9].

Eight nodes, denoted as *anchors*, are placed at the vertexes of the space during the construction (manufacturing) of network. These anchors are indexed as shown in Fig. 1 ($A_{1\ldots8}$). Note that the anchors are identical to any other node. Their uniqueness pertains to their role in the node *addressing* phase.

Node addressing phase happens once and serves as the initialization of the system. It allocates addresses to the nanonodes, which are saved for the lifetime of the network. Extending the addressing scheme of [20], we employ the 3D location of a node as its address using a trilateration process [15]. Initially, the nodes obtain their distances from the anchors as follows. The anchor A_1 initiates the addressing phase by broadcasting a data packet with the structure:

setup flag (1 bit)	anchor index (3 bits)	hop count

A *setup flag* set to the value "1" denotes that the packet is exchanged as part of the initialization phase. Additionally, the *hop count* integer field is set to 0. Each non-anchor recipient node increases the hop count field by 1 and memorizes the ensuing value as its distance from anchor $A_{anchor\,index}$. Subsequently, it re-broadcasts the packet. These steps are executed only for the first received packet from a given anchor. Should an anchor-node with index $(anchor\,index)+1$ receive such a packet (e.g., A_2), it is triggered to generate its own setup packet. A trivial timeout is used to ensure that the previous setup packet has reached all the nodes and disappeared from the network. Thus, once the initialization phase is complete, each node has obtained its address as the hop distances r_i, $i = 1 \ldots 8$, from the anchors $A_{1\ldots8}$.

Notice that several neighboring nodes are assigned the same address, In other words, an address refers to an area, denoted as *zone*, rather than a node. The fact that all nodes within a zone share the same geo-address allows for a degree of natural node fail-over. Given the frequent node failures in the nano-environment, geo-address sharing increases the chances that the network will remain connected after each failure.

Generally, a point in 3D space is uniquely identified by its distances from 4 anchor points [15]. However, the employed 3D addressing scheme can conditionally use only 3 anchors for this task. The necessary condition for unique zone identification follows.

LEMMA 2.1. *A zone can be uniquely identified by three anchors distances, $\{\dot{r},\ \ddot{r},\ \dddot{r}\}$, located at the same face of the rectangular network space.*

Proof. Assume a rectangular network space with side lengths X, Y, Z, and a Cartesian system, with $x \in [0,\ X]$, $y \in [0,\ Y]$, $z \in [0,\ Z]$. Let three anchors located on one face of the space:

$$\dot{A} = \{0,\ 0,\ 0\}\,,\ \ddot{A} = \{X,\ 0,\ 0\}\,,\ \dddot{A} = \{0,\ 0,\ Z\} \quad (1)$$

Notice that, by proper rotation and transfer, these anchors can represent any triple of vertexes on the same side of a 3D rectangle. Furthermore, let any point P within the space have Cartesian coordinates, $\{x,\ y,\ z\}$, and distances from the anchors, $\{\dot{r},\ \ddot{r},\ \dddot{r}\}$. The distances define the equations:

$$z = \sqrt{\dot{r}^2 - x^2 - y^2} \quad (2)$$

$$z = \sqrt{\ddot{r}^2 - (x - X)^2 - y^2} \quad (3)$$

$$z = Z - \sqrt{\dddot{r}^2 - x^2 - y^2} \quad (4)$$

We will show that each $\{\dot{r},\ \ddot{r},\ \dddot{r}\}$ corresponds to a unique $\{x,\ y,\ z\}$ triplet. From (2) and (3) we easily derive x uniquely as:

$$x = \frac{r^2 - \dot{r}^2 + X^2}{2 \cdot X} \quad (5)$$

z is also uniquely identified from (2) and (4) as:

$$z = \frac{\dot{r}^2 - \dddot{r}^2 + Z^2}{2 \cdot Z} \quad (6)$$

Finally, from (2) we obtain two candidate y values as:

$$y = \pm\sqrt{\dot{r}^2 - x^2 - z^2} \quad (7)$$

However, our initial assumption is that $y \in [0,\ Y]$. Thus, the negative solution can be rejected, leading to the unique definition of the complete triplet, $\{x,\ y,\ z\}$. ■

The proven property enables the linear routing scheme detailed in the ensuing Section.

3. STATELESS LINEAR ROUTING

The presented Stateless Linear Routing defines a way for routing a packet from any sender node P_1 to any recipient P_2, both identified by their addresses. The sender initially selects the *three* anchors out of $A_{1\ldots8}$ (i.e., $\{\dot{A}, \ddot{A}, \dddot{A}\}$) which act as the *coordinate system (CS)* for the packet route towards node P_2. The considerations on the anchor selection process are discussed at the end of this Section. The corresponding *usable addresses (UA)* of P_1 and P_2 are denoted as: $UA_1 : \{\dot{r}_1, \ddot{r}_1, \dddot{r}_1\}$ and $UA_2 : \{\dot{r}_2, \ddot{r}_2, \dddot{r}_2\}$. Then, the sender constructs a packet structured as:

setup flag (1 bit)	packet id (8 bits)	CS (3×3 bits)
UA_1 (var)	UA_2 (var)	DATA (var)

where *packet id* is a random integer number and *DATA* is the useful load of the packet. Any node P receiving this packet: i) checks if a packet with the same id has already been received, in which case it discards the packet. Elsewhere, the node: ii) memorizes the packet id for a trivial amount of time, in order to avoid route loops. iii) Deduces its usable address, $UA : \{\dot{r}, \ddot{r}, \dddot{r}\}$, based on the CS field. iv) Re-transmits the packet if it is located on the linear path connecting P_1 and P_2. The latter check is performed as follows.

In order to deduce whether a node P is located on the straight line, $\overline{P_1P_2}$, one should ideally convert the UAs of P, P_1, P_2 to Cartesian coordinates, and then check the compliance to the standard relation:

$$\frac{x - x_1}{x_2 - x_1} = \frac{y - y_1}{y_2 - y_1} = \frac{z - z_1}{z_2 - z_1} \tag{8}$$

However, this approach poses two challenges. First, converting UAs to Cartesian coordinates requires knowledge of the overall network space dimensions and floating point processing capabilities, as shown in equations (5)–(7). Note that the nodes are only aware of their distances from the network anchors. Deriving the network space dimensions requires extra computations with floating point precision as well.

In order to avoid the complexity challenges, we shall treat the UAs, i.e., point-to-anchor distances $P : \{\dot{r}, \ddot{r}, \dddot{r}\}$, as a curvilinear coordinate system [21]. Thus, the equation of a line connecting two points $P_1 : \{\dot{r}_1, \ddot{r}_1, \dddot{r}_1\}$ and $P_2 : \{\dot{r}_2, \ddot{r}_2, \dddot{r}_2\}$ becomes:

$$\frac{\dot{r} - \dot{r}_1}{\dot{r}_2 - \dot{r}_1} = \frac{\ddot{r} - \ddot{r}_1}{\ddot{r}_2 - \ddot{r}_1} = \frac{\dddot{r} - \dddot{r}_1}{\dddot{r}_2 - \dddot{r}_1} \tag{9}$$

This approach also justifies the focus of Lemma 2.1 to three anchors, instead of the four required by formal trilateration processes.

The second challenge for linearity check stems from the fact that the distances $\dot{r}, \ddot{r}, \dddot{r}$ measure number of hops and, therefore, are integer numbers. Thus, relation (9) will not hold precisely in the general case. To address this issue we rewrite relation (9) as:

$$\begin{cases} (\dot{r} - \dot{r}_1)(\ddot{r}_2 - \ddot{r}_1) - (\ddot{r} - \ddot{r}_1)(\dot{r}_2 - \dot{r}_1) = 0 \\ (\dot{r} - \dot{r}_1)(\dddot{r}_2 - \dddot{r}_1) - (\dddot{r} - \dddot{r}_1)(\dot{r}_2 - \dot{r}_1) = 0 \end{cases} \tag{10}$$

Subsequently, we define the quantities:

$$\mathbf{\Delta^a}(\dot{r}, \ddot{r}) = (\dot{r} - \dot{r}_1)(\ddot{r}_2 - \ddot{r}_1) - (\ddot{r} - \ddot{r}_1)(\dot{r}_2 - \dot{r}_1) \tag{11}$$

$$\mathbf{\Delta^b}(\dot{r}, \dddot{r}) = (\dot{r} - \dot{r}_1)(\dddot{r}_2 - \dddot{r}_1) - (\dddot{r} - \dddot{r}_1)(\dot{r}_2 - \dot{r}_1) \tag{12}$$

Therefore, instead of evaluating direct compliance with (9) or (10), we can simply check whether $\mathbf{\Delta^a}$, $\mathbf{\Delta^b}$ undergo a sign change when altering $\dot{r}$, $\ddot{r}$, $\dddot{r}$. Thus, we define the quantities:

$$\begin{gathered} \mathbf{\Delta^a_{\dot{r}}}(\dot{r}, \ddot{r}) = \mathbf{\Delta^a}(\dot{r} - m, \ddot{r}) \\ \mathbf{\Delta^a_{\ddot{r}}}(\dot{r}, \ddot{r}) = \mathbf{\Delta^a}(\dot{r}, \ddot{r} - m) \\ \mathbf{\Delta^a_{\dot{r}\ddot{r}}}(\dot{r}, \ddot{r}) = \mathbf{\Delta^a}(\dot{r} - m, \ddot{r} - m) \end{gathered} \tag{13}$$

$$\begin{gathered} \mathbf{\Delta^b_{\dot{r}}}(\dot{r}, \dddot{r}) = \mathbf{\Delta^b}(\dot{r} - m, \dddot{r}) \\ \mathbf{\Delta^b_{\dddot{r}}}(\dot{r}, \dddot{r}) = \mathbf{\Delta^b}(\dot{r}, \dddot{r} - m) \\ \mathbf{\Delta^b_{\dot{r}\dddot{r}}}(\dot{r}, \dddot{r}) = \mathbf{\Delta^b}(\dot{r} - m, \dddot{r} - m) \end{gathered} \tag{14}$$

where m is a non-zero integer. Thus, a node can deduce whether it is placed on a line by performing the following checks:

$$\begin{gathered} (\mathbf{\Delta^a} \cdot \mathbf{\Delta^a_{\dot{r}}} \leq 0 \quad \text{OR} \quad \mathbf{\Delta^a} \cdot \mathbf{\Delta^a_{\ddot{r}}} \leq 0 \quad \text{OR} \quad \mathbf{\Delta^a} \cdot \mathbf{\Delta^a_{\dot{r}\ddot{r}}} \leq 0) \\ \text{AND} \\ (\mathbf{\Delta^b} \cdot \mathbf{\Delta^b_{\dot{r}}} \leq 0 \quad \text{OR} \quad \mathbf{\Delta^b} \cdot \mathbf{\Delta^b_{\dddot{r}}} \leq 0 \quad \text{OR} \quad \mathbf{\Delta^b} \cdot \mathbf{\Delta^b_{\dot{r}\dddot{r}}} \leq 0) \end{gathered} \tag{15}$$

The integer m controls the "width" of the linear path, essentially introducing a way of meeting the requirement for path redundancy in nanonetworking. A value of $m = 1$ corresponds to minimal redundancy, while greater values increase the number of alternative paths. The value of m could be a global preset, or a part of the packet header set by the original sender. For example, a sender may initially choose a value of $m = 1$. If no delivery acknowledgement is received, the sender can then retry with a value of $m = 2$, etc. The redundancy introduced by m is complementary to the zone redundancy, enforced by the addressing scheme as discussed in Section 2. Zone redundancy favors network connectivity, while m introduces path redundancy by employing additional zones.

The condition (15) checks whether a node is located on a linear path of width m, defined by P_1 and P_2. Additionally, a node can check whether it is on the line *segment* connecting P_1 to P_2 based on the condition:

$$\begin{gathered} (\dot{r} - \dot{r}_2)(\dot{r} - \dot{r}_1) \leq 0 \quad \text{AND} \quad (\ddot{r} - \ddot{r}_2)(\ddot{r} - \ddot{r}_1) \leq 0 \quad \text{AND} \\ (\dddot{r} - \dddot{r}_2)(\dddot{r} - \dddot{r}_1) \leq 0 \end{gathered} \tag{16}$$

Therefore, the linear routing process, outlined as Algorithm 1, consists of: i) checking compliance with condition (16) first, and subsequently with condition (15). If any condition yields false, the packet is consumed and is not retransmitted.

Input: An incoming packet `pkt` at a node P.
Output: Retransmission decision.

1 Derive $UA : \{\dot{r}, \ddot{r}, \dddot{r}\}$ of P, from `pkt.CS`
2 $UA_1 \leftarrow$ `pkt.UA`$_1$, $UA_2 \leftarrow$ `pkt.UA`$_2$
3 $m \leftarrow$ `pkt.m`; //In case `m` is a header of `pkt`
4 **if** *Condition(16) AND Condition(15)* **then**
5 | retransmit `pkt`
6 **end**

Algorithm 1: The Stateless Linear Routing process.

Note that the described packet routing process was designed to meet the nanonetworking specifications outlined in Section 1. It inherently provides tunable path redundancy via the m parameter, which also affects the involved number of retransmitters and, hence, the expended energy. Additionally, its stateless nature (absence of routing tables) translates to minimal memory overhead. Moreover, it considers the limited nano-CPU capabilities, by requiring integer calculations only.

A consideration stemming from the anchor selection process is illustrated in the 2D example of Fig. 2. The direct mapping of curvilinear coordinates to Cartesian naturally yields curved paths (dashed lines). Should we select anchors A_1, A_2 too close to a communicating pair the curvature is high, while distant anchors yield approximately straight paths. On the other hand, the zone resolution of the addressing system is better (i.e., less nodes per zone) for medium pair-to-anchors distances (shaded areas, Fig. 2). Formally analyzing this trade-off is planned as a future extension of the present work. In the context of this study we operate heuristically and prioritize curvature reduction by

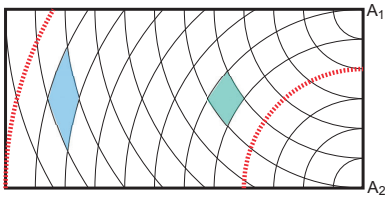

Figure 2: The path curvature and zone resolution trade-off stemming from the selection of anchors.

Table 1: Simulation Parameters.

Parameter	Value
Communication & Power Parameters	
Frequency	100 GHz
Transmission Power	5 dBnW
Noise Level	0 dBnW
Reception SINR threshold	−10 dB
Guard Interval	0.1 nsec
Packet Duration	10 nsec
Path Attenuation Parameters	
Absorption Coefficient K	0.52 dB/Km
Shadow Fading Coefficient X	0.5 dB
Space setup (Number of nodes: 5000**)**	
Cubic 1×1×1 cm, Grid/Random node placement	

selecting an anchor triplet, $\{\dot{A}, \ddot{A}, \dddot{A}\}$, on the smallest face of the rectangle space. Ties are broken arbitrarily and the selection is persistent and fixed for all node pairs.

4. SIMULATIONS

This Section evaluates the routing efficiency of the proposed Stateless Linear Routing (SLR), compared to the CORONA routing approach [20]. CORONA is a recently proposed, stateless and provenly scalable nano-routing approach. It proposes a packet flood approach, contained within the area defined by the minimal and maximal anchor distances of the communicating node-pair. Thus, although originally proposed for 2D networks, CORONA is easily extended to the 3D case as well. The main comparison metric is the communication success probability between any node pair, under the conditions of: i) failures of intermediate nodes due to energy depletion, and ii) simultaneous, potentially interfering communications taking place in parallel. The simulator is implemented on the AnyLogic platform [23], and the parameters are given in Table 1 [19].

System setup. We assume a number of $N = 5000$ nodes within a cubic 3D network space with side size 1 cm. Two layouts are studied, according to which the nodes are placed: i) on a regular grid with $1/16$ cm spacing, or ii) randomly within the space. The latter case is derived from the regular grid by deactivating a random subset of the nodes, as discussed below (run setup).

Each node represents a nano-controller in a smart meta-material application [14]. The space among the nodes is filled with air composed of standard atmospheric gases at normal humidity [5]. This dense network setup as a whole is intended to approximate the building block for a visible light-interacting smart meta-material [14].

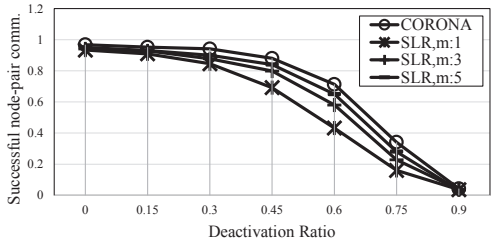

Figure 3: SLR tunability effects on the node-pair communication ratio.

Regarding the communication model, all nodes are equipped with isotropic antennas. Molecular absorption due to the air (absorption coefficient K [7]) and shadow fading (X coefficient in dB [11]) are taken into account. The Signal to Interference plus Noise (SINR) model is used to deduce the success of a packet reception [6]. The transmission power was chosen to ensure that each zone comprises approximately 15 nodes. Thus, the resolution of the network space is $7 \times 7 \times 7$ zones within a $1\,\text{cm}^3$ volume. This low resolution constitutes a *worst-case* scenario for the proposed scheme, since it hinders the formation of well-defined linear paths. The behavior in higher resolution cases is also studied at the end of this Section.

Run setup. A run is initiated by forming the described grid arrangement of nodes. A random percentage of nodes (denoted as *deactivation ratio*) is deactivated, emulating failing nodes. Thus, non-zero values of the deactivation ratio have the indirect effect of randomizing the topology as well. Then, a series of 100 operation cycles takes place, with an interarrival of 10 sec as follows. A number of nodes pairs (denoted as *pair number*) are randomly selected, each requiring the exchange of a single, unique packet. At the end of the 100 cycles, we log the percentage of pairs that communicated successfully (*comm. success ratio*). Each run is repeated 100 times, randomizing the node failures anew, to improve the confidence of the presented results in various topologies.

Results. Figures 3 and 4 illustrate the tunability of the proposed scheme (SLR) versus the related CORONA approach. The pair number is kept constant to 5, and the deactivation ratio varies from 0 to 90%. Figure 3 then shows the attained communication success ratio for various levels of SLR path redundancy (m), while Figure 4 presents the corresponding average percentage of the total network nodes serving as intermediate retransmitters per communicating pair. A higher number of retransmitters is evidence of higher energy expenditure rate. The plots in both Figures naturally decrease as the deactivation ratio increases. High deactivation rates yields segmented network areas, reducing the success ratio. Additionally, less nodes remain available to serve as retransmitters.

Notably, SLR introduces tunable success ratio and energy efficiency via the path redundancy parameter m, as described in the analysis of Section 3. In other words, SLR allows for a sender node to regulate the network energy expenditure rate, depending on its estimation for the network state. Thus, future schemes can exploit SLR to automatically employ less path redundancy (and, thus, less expense energy) when the network conditions are estimated as relatively good. On the opposite case when the network condi-

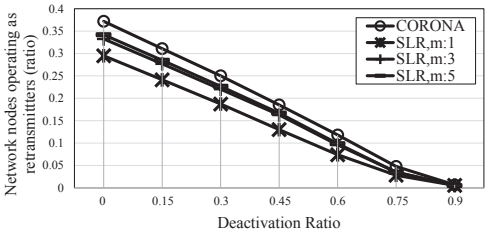

Figure 4: SLR tunability effects on the average, network-wide ratio of retransmitters serving each communicating pair.

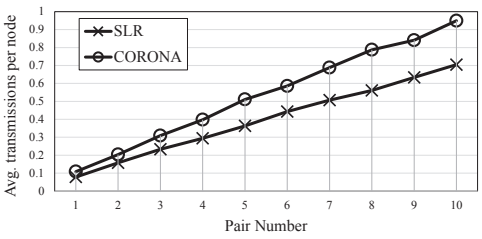

Figure 5: Average packet transmissions per node imposed by CORONA and the proposed SLR, versus the number of concurrently communicating node pairs in the network.

tions are characterized as challenging, the sender node could automatically increase m, attaining higher path diversity and communication success ratio. Mechanisms for network state estimation and automatic adaptation constitute possible extensions of the present work.

We proceed to evaluate the potential for parallel communications offered by SLR in Fig. 5. Keeping the path redundancy and deactivation ratio constant ($m = 1$ and 0% respectively), the pair number is varied in the range 1 to 10, i.e., one to ten node pairs communicating in parallel (x-axis). For each case, we measure the average number of retransmissions imposed to each network node. A higher number of retransmissions implies that the network nodes will deplete their energy reserved faster, thus yielding lower potential for parallel communications. SLR provides better performance over CORONA from this aspect, which is attributed to the well-defined, linear form of the SLR paths. On the other hand, CORONA defines much large volumes within which packet flooding is executed. Thus, it inevitably incurs more redundant transmissions per node, yielding decreased parallel communications potential.

The presented results are especially promising, given that they refer to a very small space ($1\,\mathrm{cm}^3$), where the gain margin is very limited due to the low zone resolution (cf. "system setup" above). In Fig. 6 we proceed to study the expected gains in a bigger network space with dimensions ($50 \times 50 \times 50\,\mathrm{cm}$). The network nodes are proportionally increased, yielding simulation runtime issues. Therefore, we restrict Fig. 6 to a single, indicative node-pair communication case ($m = 1$). As illustrated, the gains of SLR over CORONA increase considerably in bigger spaces. SLR yields a well-defined arc (i.e., curvilinear path). On the other hand, CORONA produces a much larger volume of restransmitters, defined by the distances of the communi-

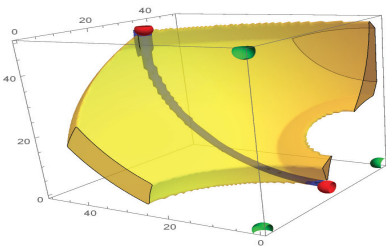

Figure 6: Comparison of CORONA (yellow area) and the novel SLR (dark curve) routing behavior for a given communicating node pair in a high-resolution space.

cating nodes from the selected anchors. Thus, CORONA trades routing area size for wider network reachability (i.e., high path redundancy), albeit without tunability potential. SLR, on the other hand, can yield very narrow, linear paths to very wide network areas, setting the basis for adaptivity in the highly challenging nano-environment.

5. RELATED WORK

Related studies on data routing within propagation focused on setups pertaining to Body Area Network (BAN) applications [18]. These networks comprise sparse, full-mesh topologies of mobile nodes. Due to their low numbers, the nodes are commonly assumed to have unique identifiers. Furthermore, BAN-oriented studies assume hierarchical networks, where a set of relatively powerful nano-routers control the smaller, weaker, cheaper nanonodes [17]. In this context, studies have focused on Medium Access Control (MAC) schemes that take into consideration the energy harvesting rate to achieve perpetual operation [1, 16]. Subsequently, energy-aware neighborhood discovery and node handshake processes are proposed in these studies. Due to the presence of the larger nano-routers, the hierarchical approach is too intrusive for the smart material applications targeted by the present study [14]. Additionally, such applications require large networks, and minimal transmission power per node, which translates to multi-hop routing requirements and non-unique addressing.

Due to their mutual emphasis on low-overhead communication, routing in nanonetworks exhibits similarities to wireless sensor networks (WSN) [25]. However, the restrictions of the nano-environment invalidate existing WSN routing solutions. It has been experimentally confirmed that well-known routing protocols, such as AODV, DSDV, or DSR are not scalable in terms of nodes or energy expenditure [12]. More lightweight geo-addressing WSN approaches provide satisfactory performance for large networks [12]. Nonetheless, such routing algorithms require directional routing, attained with neighborhood discovery, routing tables, and even memorization of past node attributes (last-seen location, direction, velocity).

Similarities also exist between routing in nanonetworks and networks-on-chips (NoCs) [24]. NoCs need to discover their topology and perform defect mapping in a completely decentralized manner [4]. Nonetheless, NoCs assume few, powerful nodes, which rely on external power supply and not on scavenging [24]. Therefore, NoC-oriented solutions are generally not portable to nanonetworks.

Regarding the authors' prior work, a ray-tracing-based simulation technique for nanonetworks was studied in [10]. Liaskos et al. proposed a metaheuristic-based, selective flooding dissemination scheme for 2D nanonetworks [13], which was later refined in terms of complexity [19]. Tsioliaridou et al. proposed a joint peer-to-peer routing and geo-addressing approach for 2D networks [20]. The routing operated via selective flooding within network sub-areas. The present paper differentiates by extending the geo-addressing scheme to 3D, and by proposing a routing approach over curvilinear paths, accomplished in a stateless manner.

6. CONCLUSION

The present study introduced a novel addressing and routing scheme for 3D electromagnetic nanonetworks, targeting Software-defined Materials (SDMs) [14]. The scheme allows for tunable routing path redundancy, in order to counter the highly lossy nature of nano-communications while limiting redundant transmissions. Additionally, it yields well-defined, linear routing paths among communicating pairs, allowing for a considerable degree of parallel transmissions within the network. The scheme is stateless, requiring no permanent memory overhead or neighborhood discovery at the nanonode-side. Limitations of nano-CPUs are also taken into account, and each routing decision requires few integer calculations only. The traits of the novel scheme were evaluated via extensive simulations. The scheme constitutes an enabling factor for SDMs, allowing for highly anticipated, future nanonetworking applications in industrial materials and ultra efficient renewable energy sources.

7. ACKNOWLEDGMENTS

This work was partially supported by the EU Horizon 2020 VirtuWind project (Grant no. 671648).

8. REFERENCES

[1] Afsharinejad, A., et al. Dynamic channel allocation in electromagnetic nanonetworks for high resolution monitoring of plants. *Nano Comm. Networks* (2015).

[2] Akyildiz, I., and Jornet, J. The Internet of nano-things. *IEEE Wireless Comm. 17*, 6 (2010), 58–63.

[3] Boillot, N., Dhoutaut, D., and Bourgeois, J. Using nano-wireless communications in micro-robots applications. In *NANOCOM'14*.

[4] Catania, V., et al. Distributed topology discovery in self-assembled nano network-on-chip. *Computers & Electrical Eng. 40*, 8 (2014), 292–306.

[5] ITU-R. Recommendation P.676-7: Attenuation by atmospheric gases, Feb. 2007.

[6] Iyer, A., Rosenberg, C., and Karnik, A. What is the right model for wireless channel interference? *IEEE Trans. on Wireless Comm. 8*, 5 (2009), 2662–2671.

[7] Jornet, J., and Akyildiz, I. Channel Modeling and Capacity Analysis for Electromagnetic Wireless Nanonetworks in the THz Band. *IEEE Trans. on Wir. Comm. 10*, 10 (2011), 3211–3221.

[8] Jornet, J., and Akyildiz, I. Joint Energy Harvesting and Communication Analysis for Perpetual Wireless Nanosensor Networks in the THz Band. *IEEE Trans. on Nanotechnology 11*, 3 (2012), 570–580.

[9] Jornet, J., Capdevila, J., and Pareta, J. A Physical Layer Aware MAC protocol for Electromagnetic nanonetworks in the THz Band. *Nano Comm. Networks 3*, 1 (2012), 74–81.

[10] Kantelis, K., et al. On the Use of FDTD and Ray-Tracing Schemes in the Nanonetwork Environment. *IEEE Comm. Letters 18*, 10 (2014), 1823–1826.

[11] Kim, S., and Zajic, A. A path loss model for 300-GHz wireless channels. In *IEEE Intl. Symposium on Antennas and Propagation* (2014), pp. 1175–1176.

[12] Lemmon, C., et al. Geographic forwarding and routing for ad-hoc wireless network. In *NCM'09*.

[13] Liaskos, C., and Tsioliaridou, A. A Promise of Realizable, Ultra-Scalable Communications at nano-Scale. *IEEE Trans. on Comp. 64* (2015), 1282–1295.

[14] Liaskos, C., Tsioliaridou, A., Pitsillides, A., Akyildiz, I., Kantartzis, N., Lalas, A., Dimitropoulos, X., Ioannidis, S., Kafesaki, M., and Soukoulis, C. Building Software Defined Materials with Nanonetworks. *IEEE Circuits and Systems Mag. 15*, 4 (2015), 12–25.

[15] Manolakis, D. E. Efficient solution and performance analysis of 3-d position estimation by trilateration. *Aerospace and Electronic Systems, IEEE Trans. on 32*, 4 (1996), 1239–1248.

[16] Mohrehkesh, S., et al. Drih-mac: A distributed receiver-initiated harvesting-aware mac for nanonetworks. *Molecular, Biological and Multi-Scale Comm., IEEE Trans. on 1*, 1 (2015), 97–110.

[17] Pierobon, M., et al. A routing framework for energy harvesting wireless nanosensor networks in the THz Band. *Wireless Networks 20*, 5 (2014), 1169–1183.

[18] Piro, G., Boggia, G., and Grieco, L. On the design of an energy-harvesting protocol stack for Body Area Nano-NETworks. *Nano Comm. Networks 6*, 2 (2015), 74–84.

[19] Tsioliaridou, A., et al. Lightweight, self-tuning data dissemination for dense nanonetworks. *Nano Communication Networks, (In Press)* (2015).

[20] Tsioliaridou, A., Liaskos, C., Ioannidis, S., and Pitsillides, A. CORONA: A Coordinate and Routing system for Nanonetworks. In *ACM NANOCOM'15*.

[21] Vinson, J. R. Curvilinear coordinate systems. In *The Behavior of Shells Composed of Isotropic and Composite Materials*. Springer, 1993, pp. 1–14.

[22] Wang, P., et al. Energy and spectrum-aware MAC protocol for perpetual wireless nanosensor networks in the THz Band. *Ad Hoc Networks 11*, 8 (2013), 2541–2555.

[23] XJ Technologies. The AnyLogic Simulator, 2013.

[24] Younis, M., et al. Topology management techniques for tolerating node failures in wireless sensor networks: A survey. *Computer Networks 58* (2014), 254–283.

[25] Yu, H., et al. Forwarding schemes for em-based wireless nanosensor networks in the thz band. In *NANOCOM' 15*.